Improved Resolution of Magnetic Resonance Microscopy in Examination of Skin Tumors

Stephan el Gammal, Roland Hartwig, Sitke Aygen,* Thomas Bauermann,* Claudia el Gammal, and Peter Altmeyer

Dermatological Clinic of the Ruhr-University Bochum, Bochum; and *Institute for "Zentrale Analytik und Strukturanalyse" of the University Witten/Herdecke, Witten, Germany

Magnetic resonance imaging has become increasingly important for visualization and tissue differentiation of internal organs. Because of limited resolution, investigation of skin has been of little diagnostic value so far. We combined a homogeneous magnetic field of 9.4 T, as used in magnetic resonance spectroscopy, with gradient fields of 11.7 G/cm and an imaging unit to obtain a voxel resolution of 40 × 40 × 300 μm^3. With this magnetic resonance microscopy unit, we studied normal skin, 12 nevocellular nevi, 20 basal cell carcinomas, 8 melanomas, and 8 seborrheic keratoses after excision *in vitro*. The specimens were visualized in spin-echo images. The proton relaxation times T1 and T2 were determined for the different skin layers and tumor tissues. Interpretation of the spin-echo images was based on comparison with the correlating histology. Epidermis, dermis, subcutaneous tissue, and hair follicle complexes could be distinguished. Stratum corneum and hairs emitted no signal. All tumors presented as distinct, signal-rich, homogeneous structures within the dark, signal-poor dermis. Their shape corresponded to their outline in the histologic sections. Buds of superficial basal cell carcinomas could be resolved. The proton relaxation times T1 and T2 were significantly different among all skin layers and tumors. Our results demonstrate that with sufficient resolution, differentiation of skin tumors is possible using magnetic resonance imaging. ***Key words: imaging techniques/proton relaxation times/magnetic resonance imaging/tumor differentiation. J Invest Dermatol 106:1287–1292, 1996***

In 1946, Bloch and Purcell *et al* independently discovered the nuclear spin resonance signal. This led to magnetic resonance (MR) spectroscopy, which is widely used for determining the molecular composition of materials based on their specific spectroscopic curves. With MR spectroscopy, the entire material is measured as integral signal, assuming an even distribution of molecules. The use of additional magnetic gradient fields makes it possible to measure selectively within small volumes of a specimen. With magnetic resonance imaging (MRI), the specimen is analyzed in slices, and the qualities of the received signal within the voxel (volume element) are presented as gray-level modulation of one pixel (picture element) in the 2-dimensional image. Since the publication of a study on a section of water-filled capillaries by Lauterbur (1973), MRI has evolved into a potent technique to display the morphology of internal organs. Quantitative information about the composition of tissues is obtained by measuring their proton relaxation times, T1 and T2. These values are mainly determined by the water content and the interaction of water protons with macromolecules (Longmore, 1989).

The extent to which the proton relaxation times allow differentiation of tissue components depends on the resolution power of the MR image. Current MR tomographs for clinical applications use a homogeneous magnetic field between 0.23 and 2.4 T and work with magnetic gradient fields of up to 1 G/cm. At best, voxel resolutions of 5 × 5 × 5 mm^3 can be obtained (Kuhn, 1990). To examine skin *in vivo*, several researchers have improved this resolution using surface gradient coils (Hyde *et al*, 1987; Querleux *et al*, 1988; Zemtsov *et al*, 1989; Bittoun *et al*, 1990; Richard *et al*, 1991; Querleux, 1995). Thus, epidermis, dermis, and subcutis could be differentiated (Querleux *et al*, 1988; Bittoun *et al*, 1990; Richard *et al*, 1991; Querleux, 1995); however, significant tumor differentiation by measuring relaxation times was not possible (Zemtsov *et al*, 1989, 1991).

We combined a strong, homogeneous magnetic field of 9.4 T, as used in MR spectroscopy, with gradient fields of 11.7 G/cm and an imaging unit to obtain a voxel resolution of 40 × 40 × 300 μm^3. With this MR microscopy unit, we visualized different skin tumors and determined their proton relaxation times.[1] Because the construction of this strong homogeneous magnetic ground field and high gradient fields is at present technically difficult for greater volumes, with our equipment small living animals can be studied *in vivo*, whereas human skin must be investigated *in vitro*.

MATERIALS AND METHODS

Tissue Processing We investigated 12 nevocellular nevi, 20 basal cell carcinomas, 8 melanomas, and 8 seborrheic keratoses. These specimens were excised for therapeutic reasons from patients at the dermatologic clinic of the Ruhr-University Bochum. All patients gave informed consent. Ten

Manuscript received September 14, 1995; revised February 10, 1996; accepted for publication February 21, 1996.

Reprint requests to: Dr. Stephan el Gammal, Department of Dermatology, Gudrunstraße 56, D-44791 Bochum, Germany.

[1] Aygen S, el Gammal S, Bauermann T, Hartwig R, Altmeyer P: Tissue characterization of human skin tumors using MR-microscopy at 9.4 Tesla. *12th Annual Meeting of the Society of Magnetic Resonance in Medicine* 2:942, 1993 (abstr.).

Table I. T1 Relaxation Values[a]

Tissue Type	Mean Value (ms)	Standard Deviation	n
Subcutis	455.1	32.4	46
Dermis	1087.9	29.3	48
Epidermis	1152.7	32.8	28
Nevocellular nevus	1309.0	22.5	12
Seborrheic keratosis	1417.0	68.9	6
Melanoma	1445.6	130.7	7
Basal cell carcinoma	1801.2	41.4	17

[a] T1 relaxation values are significantly different among all tissues except for the values of melanoma *versus* seborrheic keratosis.

Table II. T2 Relaxation Values[a]

Tissue Type	Mean Value (ms)	Standard Deviation	n
Dermis	19.2	1.0	38
Epidermis	23.3	0.8	23
Seborrheic keratosis	24.6	0.6	5
Nevocellular nevus	26.4	0.4	8
Basal cell carcinoma	27.4	0.8	9
Melanoma	34.3	3.1	8
Subcutis	48.6	1.4	37

[a] T2 relaxation values are significantly different among all tissues

specimens of normal skin from various body regions were examined; the tissue was obtained from healthy skin within the security margin of excised high-risk melanomas.

The tissue was first thoroughly rinsed in 0.9% NaCl solution to remove blood remnants, which influence the magnetic resonance signal because of the ferromagnetic effect of hemoglobin (Wehrli, 1988). After fixation in formalin 5% for 30 min, the tissue blocks were patted dry with gauze and placed in the center of a 10-mm proton-radiofrequency (RF) coil. Examination was performed with an MR spectroscopy unit (AM 400 WB NMR; Bruker GmbH, Rheinstetten, Germany) equipped with an advanced microimaging accessory. Each tissue block was analyzed in slices. A single slice was 300 μm thick (slice thickness = selective pulse width/gyromagnetic ratio $\times$ gradient strength).

After MR imaging, the tissue was fixed in formalin for another 12-24 h and embedded in paraffin. To obtain histologic sections exactly correlating with the MR images, we cut the paraffin blocks in the same plane in which the MR images were taken. In steps of 150 μm, several 7-μm sections were cut, stained with hematoxylin and eosin, and examined under a light microscope. This procedure allowed choosing between two sets of 150-μm distant histologic sections for correlation with each 300-μm-thick MRI slice.

MR Microscopy The MR microscopy unit (Bruker AM 400 WB NMR) works with a helium-cooled supraconducting magnetic coil of 9.4 T and three orthogonal gradient coils that produce linear gradient fields of up to 75 G/cm. In a 1-cm^3 tissue block, a resolution of up to 20 μm can theoretically be achieved in the x/y-plane. We used the following imaging techniques for our investigations (Kuhn, 1990): spin-echo sequence for single and multi-slices, inversion-recovery sequence to determine the longitudinal relaxation time T1, and multi-echo sequence to determine the transverse relaxation time T2.

Spin-Echo Sequence For single-slice imaging, we used the spin-echo sequence XYIMAGE.AU (Bruker), which is based on the pulse sequence of Hahn for the generation of spin-echo images (Hahn, 1950). For multi-slice imaging, the stimulation sequence with slice-selective pulses was combined in such a way that overlap effects were kept to a minimum. While one already stimulated slice relaxed, another was stimulated. This allowed a more efficient use of the extinction time periods, which occur because the nuclei have to relax completely in longitudinal magnetization before stimulation (Kuhn, 1990).

Longitudinal Relaxation Time T1 We determined the relaxation time T1 (speed with which the longitudinal magnetization returns to its resting value after stimulation with a 180° pulse) using the inversion-recovery sequence in regions of interest of 0.01 mm^2. A 180° pulse oriented the magnetization sum vector in z-direction. To measure the amplitude of this fading vector, a 90° pulse was emitted after a defined time (inversion time), turning the magnetization sum vector into the x/y-plane. The received signal was used for gray-level modulation. By evaluating the mean gray value within the same area (corresponding to the amplitude of the magnetization sum vector in a particular direction) of eight images registered at different inversion times, a tissue-specific T1-relaxation curve was plotted.

Transverse Relaxation Time T2 As in the spin-echo imaging technique, a 180° pulse was superimposed on a previously applied 90° pulse. A spin-echo signal was emitted during refocusing. To obtain an increasing T2 weighting in multi-echo images, the 180° pulse was emitted repeatedly several times after the echo time. T2 values were calculated from a sequence of T2-weighted images (16 images from one section); the region of interest was 0.01 mm^2.

T1 and T2 values could be obtained only from a part of the specimens, as the technical setup for their measurement was not available from the very beginning of our study. **Tables I** and **II** show the numbers to which the mean values in each tissue refer.

Statistics The U-test (Mann-Whitney-Wilcoxon) for unpaired observations was used to compare the respective T1 and T2 values of different tissues (epidermis, dermis, subcutis, nevocellular nevus, melanoma, basal cell carcinoma, seborrheic keratosis); p values of ≤ 0.001 were considered significant.

RESULTS

Spin-Echo Images Correlate Exactly With the Corresponding Histology

Epidermis, Dermis, Subcutis, and Hair Follicle Complexes Can Be Differentiated In specimens of normal skin, the epidermis was represented as a narrow signal-intense band, sharply demarcated from the underlying dermis (**Fig 1*a*** and ***b***). In two cases, no signal was emitted from the skin surface; histologically they showed an atrophic epidermis with a flat dermoepidermal junction (lower leg of a 52-year-old man; back of the hand of a 47-year-old man). The dermis appeared dark, with irregularly scattered lighter spots. Hair follicles and sebaceous glands were signal rich (longitudinal structures in **Fig 1*a***). Sweat glands and nerves could be detected only in exceptional cases. Occasionally, filled blood vessels were seen as black holes. The subcutaneous fat with its dark connective tissue septa was the most signal-intense tissue.

The Hyperkeratotic Horny Layer of Seborrheic Keratoses Emits No Signal in the Spin-Echo Image All investigated seborrheic keratoses were histologically of the hyperkeratotic type. The histologically thickened stratum corneum was invisible in the spin-echo images. The laciniform acanthotic epidermis was represented as a broad white band. Round, dark exclusions in this band correlated with keratin pseudocysts in the histologic sections (**Fig 2*a*** and ***b***).

Buds of Superficial Basal Cell Carcinomas Are Visualized Histologically, 12 of the samples were superficial and 8 were solid basal cell carcinomas. The spin-echo images of superficial basal cell carcinomas showed an upper light zone, corresponding histologically to the epidermis, from which several small, round, light globules projected into the dark dermis underneath, representing buds of deeply basophilic basal cell carcinoma cells (**Fig 3*a*** and ***b***). In solid basal cell carcinomas, larger light, mostly ovoid regions were present beneath the upper light band, corresponding histologically to tumor cell nests.

Nevocellular Nevi are Signal Rich Seven nevocellular nevi were histologically of the papillomatous dermal type, and five were compound nevi. All nevi presented as signal-rich structures in the spin-echo images. Their outlines corresponded to the histology. In **Fig 4*a*** and ***b***, a papillomatous dermal nevus is shown. The dense aggregation of nevus cells in the upper dermis (**Fig 4*b***) is visible as

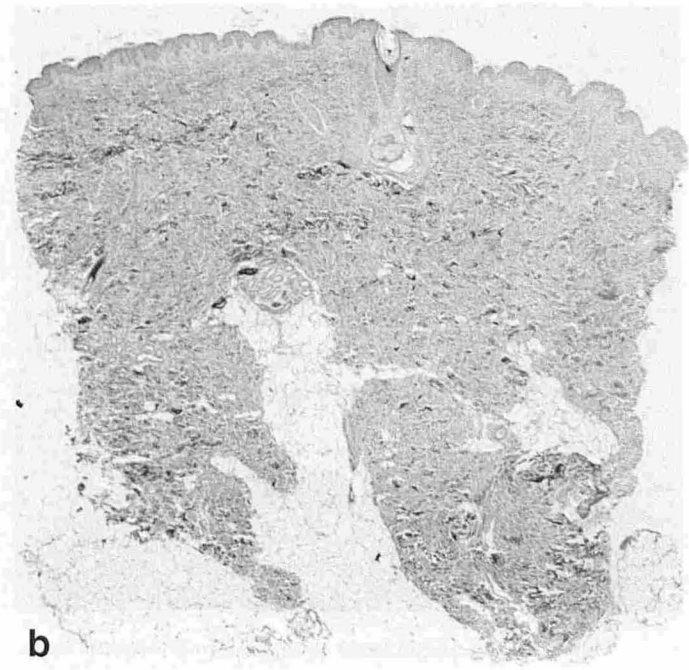

Figure 1. Normal skin from the upper leg of a 25-year-old man. *a*, spin-echo image; *b*, corresponding histology.

a broad white band in the spin-echo image **(Fig 4*a*)**. Indentations in the epidermis filled with retained horny material are represented as indentations of the upper edge of the white band; the keratin itself is not visible in the spin-echo image. The signal-rich nevus extends into the dermis along a dilated hair follicle with a longitudinally cut hair, represented as a dark loop, inside.

Melanomas Are Signal Rich; the Inflammatory Infiltrate Is Signal Poor Histologically, five of the melanomas were of the superficial spreading type, and three were primary nodular melanomas. The tumor thicknesses according to Breslow ranged from 0.9 to 4.7 mm. In the spin-echo images, all melanomas were signal rich. Their outlines corresponded to the histologic picture. Often the concomitant inflammatory infiltrate was visible as a dark sickle between the tumor tissue and the surrounding dermis, facilitating delineation of the tumor. In **Fig 5*a*** (spin-echo image) and ***b*** (histology), a primary nodular melanoma with a histologic tumor thickness of 1.65 mm is shown. The tumor is visible in the right upper part. In the spin-echo image, it is represented as a light, ovoid area with a finely granular structure. The dark dermis contains several light areas, which correlate histologically to a hair follicle and eccrine sweat glands.

Relaxation Times T1 and T2 Are Significantly Different Among All Skin Layers and Tumors **Figure 6** illustrates the determination of the T1 relaxation time, and **Table I** and **Fig 7** display the values. The subcutis had by far the lowest T1 value, at 455 ms, followed by the dermis (about 1090 ms), epidermis, nevocellular nevus, seborrheic keratosis, melanoma, and basal cell carcinoma (about 1800 ms). Standard deviations were consistently very low. T1 values were significantly different among all tissues (p

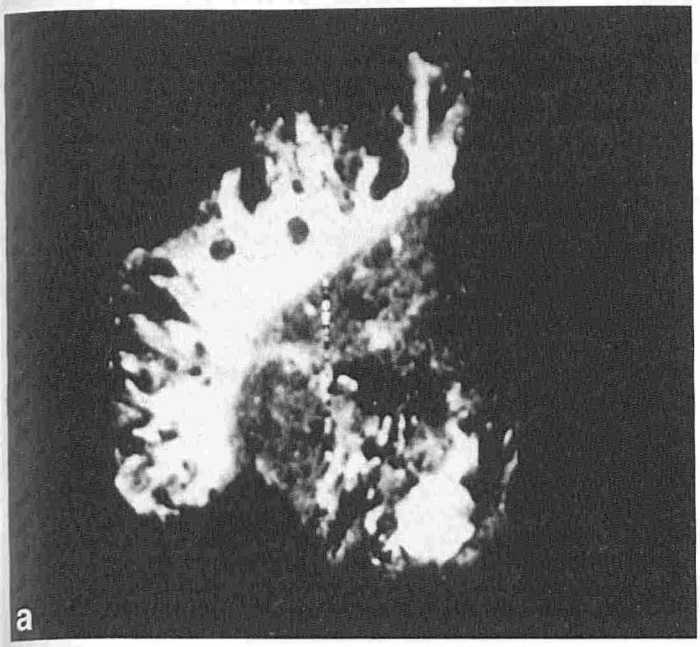

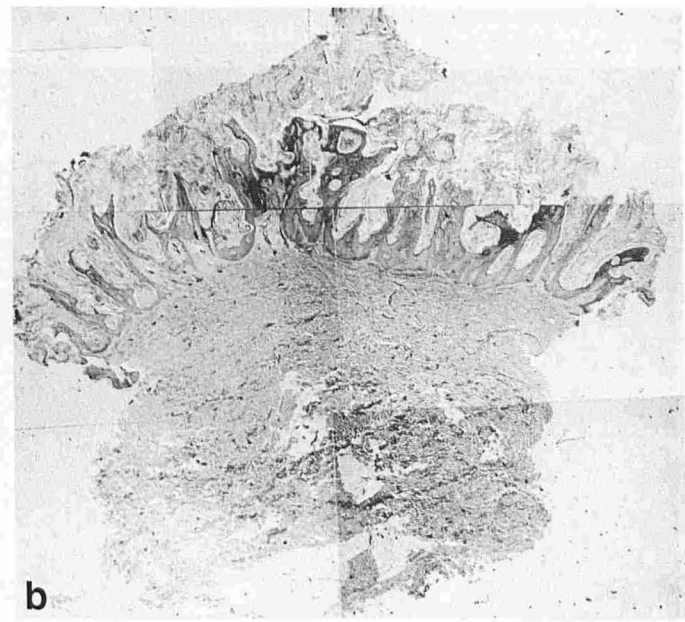

Figure 2. Seborrheic keratosis from the back of a 76-year-old woman. *a*, spin-echo image; *b*, corresponding histology.

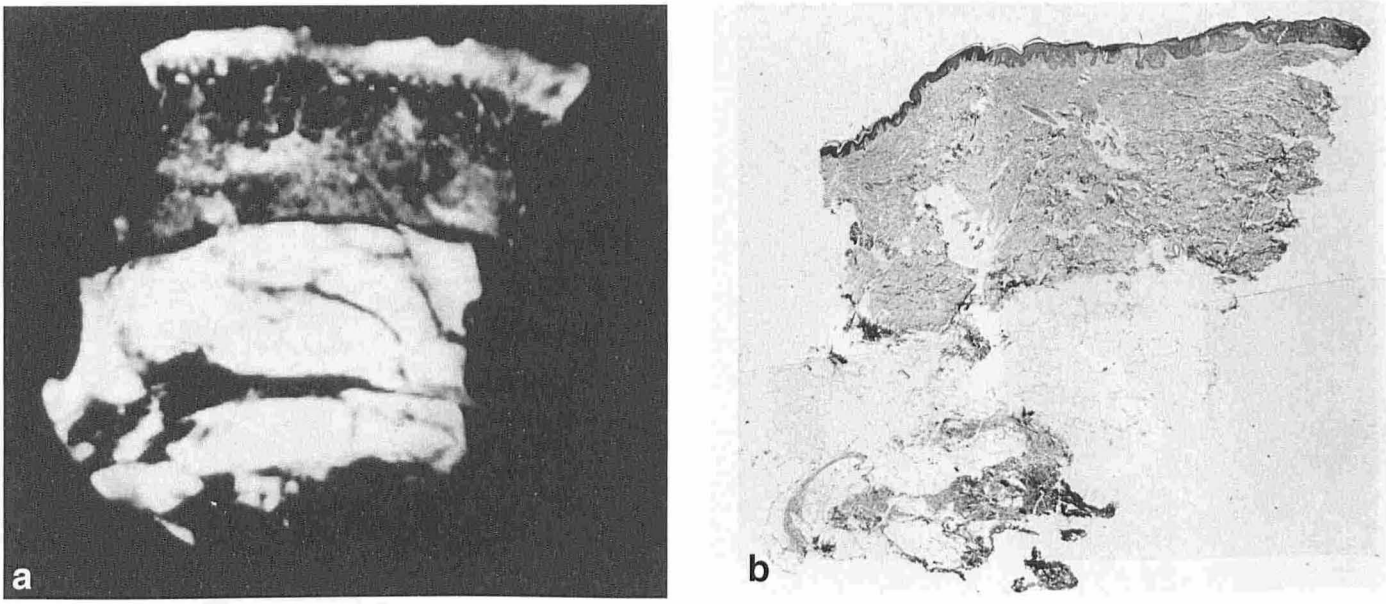

Figure 3. Superficial basal cell carcinoma from the back of an 81-year-old man. *a*, spin-echo image; *b*, corresponding histology.

< 0.001), except for the values of melanoma *versus* seborrheic keratosis.

Table II and **Fig 7** show the mean T2 relaxation times. The sequence was different from that of the T1 values: The dermis had the lowest value, at 19 ms, followed by the epidermis, seborrheic keratosis, nevocellular nevus, basal cell carcinoma, and melanoma. The subcutis showed the highest value, at 48.5 ms. T2 values were significantly different among all tissues ($p < 0.001$). The T2 values of seborrheic keratosis and melanoma did not overlap.

DISCUSSION

Because of the high resolution of $40 \times 40 \times 300\ \mu m^3$, we were able to visualize the different skin layers, skin appendages, and tumors. As the thickness of the MR slices was 300 μm, structures appeared more blurred than in the 7-μm-thick histologic sections. We found that stratum corneum and hairs emitted no signal in MR microscopy. This effect is probably due to the low water content and relative proton deficiency of keratin.

Richard *et al* (1991), using a whole-body Sigma imaging system operating at 1.5 T with a special surface gradient coil, were able to differentiate the epidermis of the calf *in vivo* as a thin, light line overlying the dark dermis. In MR images from the heel, they found two layers of different signal intensity on the surface: an outer gray and an inner brighter layer. Their interpretation—that the outer layer corresponds to the stratum corneum whereas the light one represents the living epidermis—seems plausible, although it lacks histologic verification. Salter *et al* (1992) investigated normal skin from the fingerpad using a 2-T magnetic field combined with a 20-cm-diameter gradient set. From studies of the skin at different hydration states (after immersion of the finger in water), they concluded that the living epidermis is signal intense in MR images, whereas the stratum corneum becomes visible only when it is hydrated. Similar results were obtained by Querleux (1995) on the heel. The results from these *in vivo* investigations correlate well with our *in vitro* findings. They all support the evidence that horny

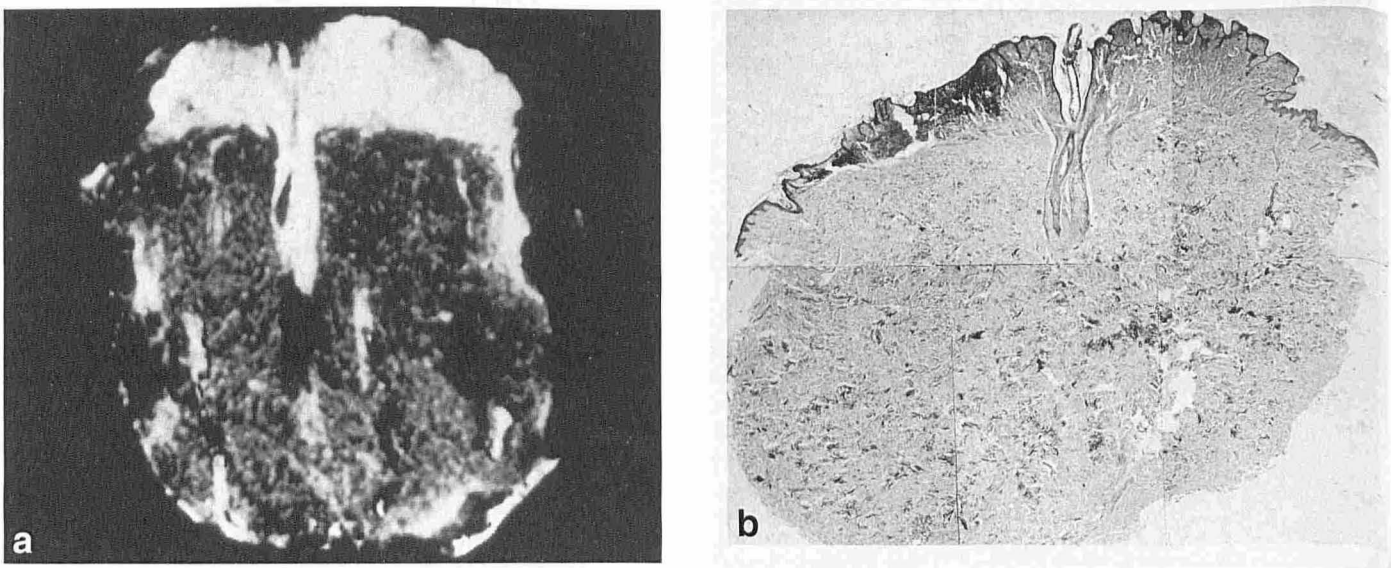

Figure 4. Papillomatous dermal nevocellular nevus from the back of a 25-year-old man. *a*, spin-echo image; *b*, corresponding histology.

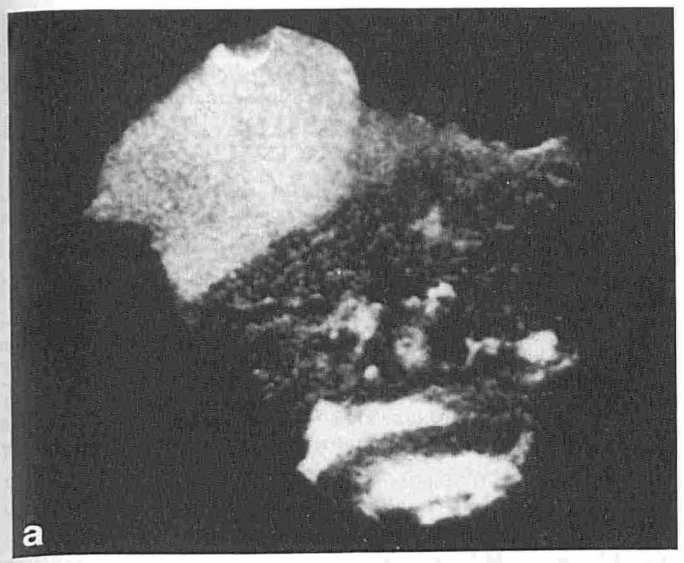

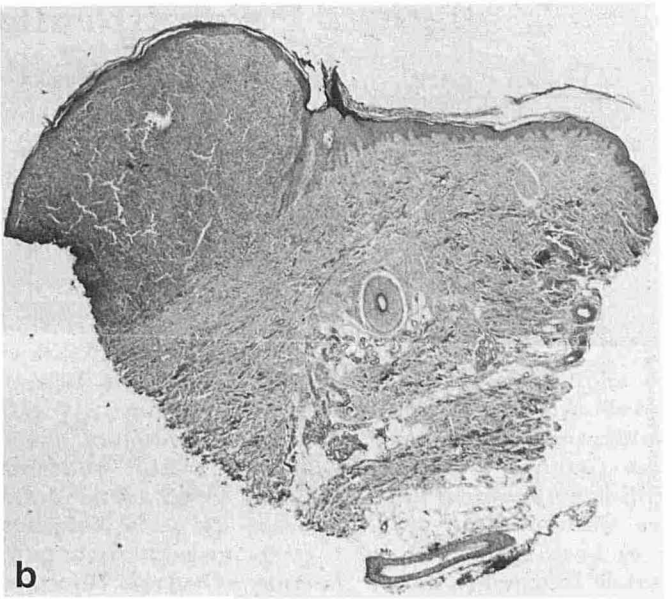

Figure 5. Primary nodular melanoma from the leg of a 31-year-old woman. Tumor thickness according to Breslow was 1.65 mm. *a*, spin-echo image; *b*, corresponding histology.

material, when dry, is signal poor and thus dark in spin-echo images, whereas the living epidermis is signal rich.

The high resolution of our MR images and the verification of structures using histology made it possible to determine the proton relaxation times precisely within the different skin layers and tumors in a region of interest of $100 \times 100\ \mu m^2$. By far the lowest T1 and highest T2 values were measured in the subcutis, as found in previous studies (Bittoun *et al*, 1990; Richard *et al*, 1991). Dooms *et al* (1986) proved the constancy of T1 and T2 values in adipose tissue on a group of 78 patients. They proposed to use the subcutis as a reference tissue in MR imaging. Richard *et al* (1991) found that T2 values of the epidermis were significantly higher than those of the dermis, consistent with our results. Divergent from our study, however, they could not establish any difference regarding T1 values.

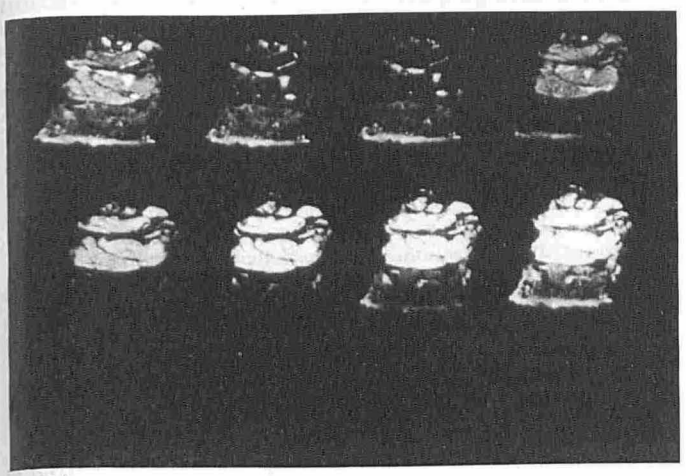

Figure 6. Basal cell carcinoma at eight different inversion times. For technical reasons, pictures were obtained upside down. Epidermis, dermis, and subcutaneous tissue go at different times through the "dark point" (intersection point of their tissue-specific T1-relaxation curve with the abscissa). In the third picture of the eight-image sequence, the subcutis is running through the dark point, whereas the dermis and epidermis have the same lightness as in the spin-echo image. In the seventh picture, epidermis and dermis are not visible because of an amplitude of zero for the z-magnetization, whereas the subcutis, which has already fully relaxed, appears as a light region. The last picture of the image sequence shows all tissue components in complete relaxation. By determining the intensity of the signal in the same picture location at different inversion times, we plotted a tissue-specific relaxation curve and calculated the absolute T1-relaxation time. In this specimen, we found a longitudinal relaxation time of 1783 ms for the tumor tissue, of 1030 ms for the dermis, and of 437 ms for the subcutaneous fat.

We found significant differences in relaxation times among the investigated skin tumors. Schwaighofer *et al* (1989) studied melanomas *versus* benign pigmented skin lesions (nevi relative to seborrheic keratoses) *in vivo* with MRI. They observed that all skin tumors were less signal intense than fat on T1-weighted images, whereas on T2-weighted images, melanomas were more signal intense and benign tumors were more signal poor than fat. Because the signal intensity of structures on T1- and T2-weighted images depends on the inversion time, however, these results represent subjective impressions rather than quantitative data. Measurements of proton relaxation times, allowing objective evaluation of tissues, were not provided.

Other researchers have denied that a significant discrimination of skin tumors is possible using relaxation times (Mafee *et al*, 1986; Zemtsov *et al*, 1989). The reasons for these difficulties in tissue differentiation are the insufficient resolution due to relatively low ground and gradient fields and the lacking histologic correlation. Moreover, most researchers took sequences of only two to eight T1- or T2-weighted images to determine the relaxation times (Dooms *et al*, 1986; Schwaighofer *et al*, 1989; Richard *et al*, 1991). The use of up to 16 images in our study rendered greater accuracy at the cost of very long image acquisition times. The inversion-recovery experiment, in particular, needed several hours. To delay autolytic processes, which prolong the T1 and T2 times (Grodd and Schmitt, 1983), we briefly fixed the specimens before the measurement. It has been described, however, that fixation influences the relaxation times as well, causing a decrease in T1 time (Grodd and Schmitt, 1983).

Apart from MRI, several other imaging methods for visualization of the skin have been developed recently. Probably the most important is high-frequency sonography, with a resolution between 40 and 200 μm. As opposed to MRI, tissue differentiation is not possible using 20-50 MHz ultrasound (Hoffmann *et al*, 1992; el Gammal *et al*, 1993; Serup *et al*, 1995). To be visualized in sonography, structures have to reflect a fraction of the applied energy. This is typically the case for the collagen bundles of the dermis, which appear as irregular white (echo-rich) spots in the

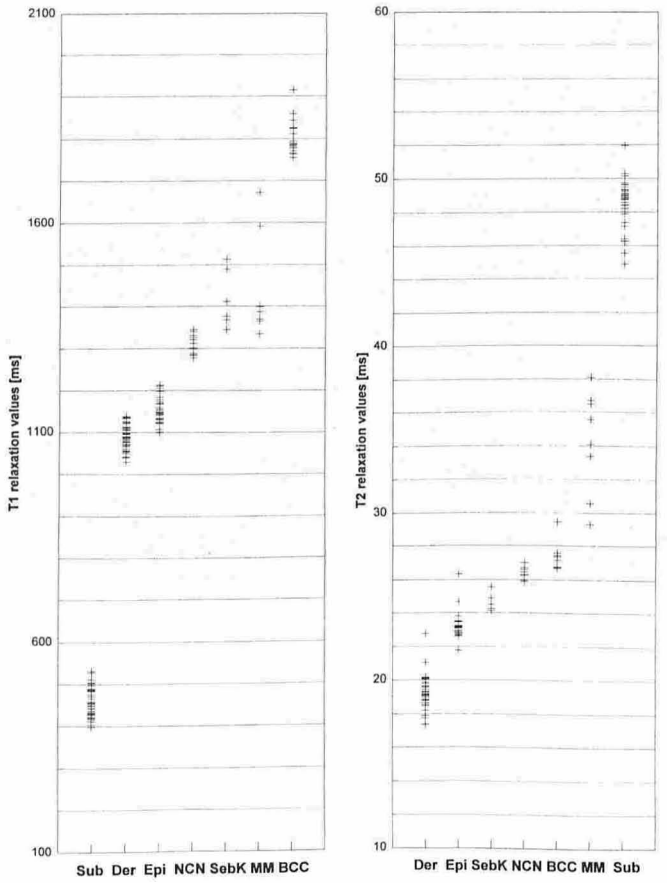

Figure 7. T1 and T2 relaxation values. *Sub*, subcutis; *Der*, dermis; *Epi*, epidermis; *NCN*, nevocellular nevus; *SebK*, seborrheic keratosis; *MM*, melanoma; *BCC*, basal cell carcinoma.

sonographic image. Inflammatory infiltrates, scar tissue, edema, and various epithelial, vascular, and melanocytic tumors, however, all appear dark (echo-poor) (el Gammal *et al*, 1994). The value of sonography lies in the differentiation of these processes from the surrounding dermis and determination of their size.

Our results show the potency of MRI for investigation of the skin. We demonstrated that the accuracy of tissue differentiation is mainly a question of resolution. With the MRI unit used in this study, we achieved a markedly higher resolution than reported in previous investigations, but our equipment is still far from being suitable for routine use. The main disadvantage is that only very small objects can be studied, and therefore the investigation of human skin must be performed *in vitro*. In the future, the development of MR microscopy systems using strong local surface coils and gradient fields placed directly on the skin might provide an important noninvasive diagnostic tool in dermatology.

REFERENCES

Bittoun J, Saint-Jalmes H, Querleux BG, Darrasse L, Jolivet O, Idy-Peretti I, Wartski M, Richard SB, Leveque JL: *In vivo* high-resolution MR imaging of the skin in a whole-body system at 1,5 T. *Radiology* 176:457-460, 1990

Bloch F: Nuclear induction. *Phys Rev* 70:460-474, 1946

Dooms GC, Hricak H, Margulis AR, de Geer G: MR imaging of fat. *Radiology* 158:51-54, 1986

el Gammal S, Auer T, Hoffmann K, Matthes U, Hammentgen R, Altmeyer P, Ermert H: High-frequency ultrasound: a noninvasive method for use in dermatology. In: Frosch PJ, Kligman AM (eds.). *Noninvasive Methods for the Quantification of Skin Functions*. Springer Verlag, Berlin, 1993, pp 104-129

el Gammal S, Auer T, Popp C, Hoffmann K, Altmeyer P, Passmann C, Ermert H: Psoriasis vulgaris in 50 MHz B-scan ultrasound—characteristic features of stratum corneum, epidermis and dermis. *Acta Derm Venereol Suppl (Stockh)* 186:173-176, 1994

Grodd W, Schmitt WGH: Protonenrelaxationsverhalten menschlicher und tierischer Gewebe *in vitro*, Änderungen bei Autolyse und Fixierung. *Fortschr Röntgenstr* 139:233-240, 1983

Hahn EL: Spin echoes. *Phys Rev* 80:580-594, 1950

Hoffmann K, Jung J, el Gammal S, Altmeyer P: Malignant melanoma in 20 MHz B scan sonography. *Dermatology* 185:49-55, 1992

Hyde JS, Jesmanowicz A, Kneeland JB: Surface coil for MR imaging of the skin. *Magn Reson Med* 5:456-461, 1987

Kuhn W: NMR microscopy—fundamentals, limits and possible applications. *Angew Chem Int Ed Engl* 29:1-19, 1990

Lauterbur PC: Image formation by induced local interactions—examples employing nuclear magnetic resonance. *Nature* 242:190-191, 1973

Longmore DB: The principles of magnetic resonance. *Br Med Bull* 45:848-880, 1989

Mafee MF, Pegman GA, Grisolano JE, Fletcher ME, Spigos DG, Wehrli FW, Rasouli F, Capek V: Malignant uveal melanoma and simulating lesions: MR imaging evaluation. *Radiology* 160:773-780, 1986

Purcell EM, Torrey HC, Pound RV: Resonance absorption by nuclear magnetic moments in a solid. *Phys Rev* 69:37-38, 1946

Querleux B: Nuclear magnetic resonance (NMR) examination of the epidermis *in vivo*. In: Serup J, Jemec GBE (eds.). *Handbook of Non-Invasive Methods and the Skin*. CRC, Boca Raton, FL, 1995, pp 133-139

Querleux B, Yassine MM, Darrasse L, Saint-Jalmes H, Sauzade M, Leveque JL: Magnetic resonance imaging of the skin. A comparison with the ultrasonic technique. *Bioeng Skin* 4:1-14, 1988

Richard S, Querleux B, Bittoun J, Idy-Peretti I, Jolivet O, Cermakowa E, Leveque JL: *In vivo* proton relaxation times analysis of skin layers by magnetic resonance imaging. *J Invest Dermatol* 97:120-125, 1991

Salter DC, Hodgson RJ, Hall LD, Carpenter TA, Ablett S: Moisturization processes in living human skin studied by magnetic resonance imaging microscopy. *IFSCC Yokohama, Japan*, 1992, pp 587-595

Schwaighofer BW, Fruehwald FXJ, Pohl-Markl H, Neuhold A, Wicke L, Landrum WL: MRI evaluation of pigmented skin tumors. *Invest Radiol* 24:289-293, 1989

Serup J, Keiding J, Fullerton A, Gniadecka M, Gniadecki R: High-frequency ultrasound examination of skin: introduction and guide. In: Serup J, Jemec GBE (eds.). *Handbook of Non-Invasive Methods and the Skin*. CRC, Boca Raton, FL, 1995, pp 239-256

Wehrli FW: Principles of magnetic resonance. In: Stark DD, Bradley WG (eds.). *Magnetic Resonance Imaging*. CV Mosby, St. Louis, 1988, pp 3-23

Zemtsov A, Lorig R, Bergfield WF, Bailin PL, Ng TC: Magnetic resonance imaging of cutaneous melanocytic lesions. *J Dermatol Surg Oncol* 15:854-858, 1989

Zemtsov A, Lorig R, Ng TC, Xue M, Bailin PL, Bergfeld WF, Larson K, Yetman R: Magnetic resonance imaging of cutaneous neoplasms: clinicopathologic correlation. *J Dermatol Surg Oncol* 17:416-422, 1991